

Article

PbMoO₄ Synthesis from Ancient Lead and Its Single Crystal Growth for Neutrinoless Double Beta Decay Search

Arshad Khan ¹, Pabitra Aryal ¹, Hongjoo Kim ^{1,*}, Moo Hyun Lee ^{2,3} and Yeongduk Kim ^{2,3}

¹ Department of Physics, Kyungpook National University, Daegu 41566, Korea; kxanarshadmsc85@gmail.com (A.K.); shpbi@gmail.com (P.A.)

² Center for Underground Physics, Institute for Basic Science (IBS), Daejeon 34126, Korea; mhlee@ibs.re.kr (M.H.L.); ydkim@ibs.re.kr (Y.K.)

³ IBS School, University of Science and Technology (UST), Daejeon 34113, Korea

* Correspondence: hongjoo@knu.ac.kr

Received: 31 January 2020; Accepted: 26 February 2020; Published: 27 February 2020



Abstract: A powder synthesis of PbMoO₄ (PMO) from ancient lead (Pb) and deeply purified commercial MoO₃ powders was performed using a wet chemistry technique to achieve the low radioactivity scintillator for neutrinoless double beta decay search in ¹⁰⁰Mo. The synthesized powders were used to grow single crystals of PbMoO₄ by the Czochralski technique in an Ar environment. The luminescence and scintillation properties were measured with excitations using UV, X- and γ -rays in the temperature range of 10–300 K. Annealing of the grown PMO crystal in an air atmosphere significantly enhanced the scintillation light yield compared to that measured before annealing. The scintillation light yield of grown PMO crystal at 10 K was found to be 127% to that of a reference PMO crystal under 662 keV γ -rays excitation from a ¹³⁷Cs source. The background measurement of the grown crystal performed at 50 K shows a lower internal activity from ²¹⁰Pb compared to that of reference PMO (grown from modern Pb) crystal. These preliminary performances show that the PMO crystal grown from ancient Pb and deeply purified MoO₃ powders has a great potential to be used as a cryogenic scintillator for the neutrinoless double beta decay search in ¹⁰⁰Mo.

Keywords: ancient Pb; synthesis; single crystal growth; scintillation; thermally stimulated luminescence

1. Introduction

PbMoO₄ (PMO) is one of the most extensively studied materials because of its wider applications in acousto-optics [1], optoelectronics [2], photocatalysis [3], and high voltage measuring devices. Single crystal growth of PMO by Czochralski technique was reported elsewhere in [4–9]. The difficulties arisen during crystal growth from bubble formation [10], compositional changes due to evaporation of the volatile MoO₃ powders [11], cracking of the crystal during and after growth and coloration, which deteriorates the optical quality of the crystal, were extensively studied and reported [12,13]. Moreover, the crystal growth with improved optical quality was reported by the low thermal gradient Czochralski technique [7].

The PMO crystal belongs to the scheelite structure of the tetragonal crystal system with the space group I4₁/a [14]. Single crystals belonging to the scheelite structure have been widely studied due to their common luminescence features for the applications in high energy physics, dark matter, and double beta decay searches [15–20]. The interest in the application of molybdate single crystalline scintillators came from the introduction of cryogenic phonon scintillation detectors (CPSD) in the search for neutrinoless double beta ($0\nu\beta\beta$) decay. Advantages of CPSD over other detectors are good

particle discrimination capability and high energy resolution [21,22]. This detection technique is under usage by AMoRE [22] and CUPID-Mo [23] experiments for the $0\nu\beta\beta$ decay search in ^{100}Mo . These experiments used $^{40}\text{Ca}^{100}\text{MoO}_4$ and $\text{Li}_2^{100}\text{MoO}_4$ (LMO) cryogenic scintillators. However, because of the purification limitation of Ca and low light output of LMO, the search for novel scintillators with improved scintillation performance, low internal background, and capability that can be grown easily in large volumes is highly desired [24]. The scintillation performance tests of PMO crystals were carried out to check the feasibility, especially for $0\nu\beta\beta$ decay searches [17,19,20]. However, the intrinsic background imposed by ^{210}Pb in the PMO crystal grown from commercial precursors limits its applications in rare event search experiments [20]. This intrinsic background can be reduced by utilizing the ancient Pb for the powder synthesis and hence PMO crystal growth. The low radioactivity archeological Pb was used to synthesize PbO powders and mixed with MoO_3 powders for the growth of PMO crystal by the low thermal gradient Czochralski technique [7]. Scintillation bolometric performance of this archeological PMO showed an excellent performance, however, it suffered from huge internal radioactivity due to the dropping of a ceramic piece during crystal growth [18]. Therefore, careful handling during powder synthesis and crystal growth is required to avoid this and other possible issues.

This study focuses on the powder synthesis of PMO directly from an ancient Pb and commercial and deeply purified MoO_3 powders by a wet chemistry technique for the first time. Two different batches of synthesized powders (i.e., from (i) ancient Pb and commercial MoO_3 , (ii) ancient Pb and deeply purified MoO_3) were used to grow two different crystals of PMO by the Czochralski technique in Ar atmosphere. Phases of the grown PMO crystals were confirmed by powders using x-ray diffraction analysis. In order to study the temperature dependent luminescence properties of the PMO crystal in the region of the direct creation of excitons, excitation energy above the band gap while lower than the ionization threshold is required [25]. The bandgap of PMO was reported to be 3.3 eV [26], therefore an excitation source having an energy of 4.42 eV was selected for a comparative luminescence analysis of the grown PMO crystals. The scintillation performance of the PMO crystal grown from powders synthesized from ancient Pb and deeply purified MoO_3 powders was studied under γ -ray excitation in the temperature range of 10–300 K and compared with a reference PMO crystal. Moreover, the effect of annealing in air atmosphere on the scintillation properties of the grown crystal was studied under γ -ray excitation. Thermally stimulated luminescence (TSL) measured after x-ray irradiation at 10 K shows multiple traps, which causes quenching of light yield at low temperatures due to the self-trapping of electrons at $(\text{MoO}_4)^{2-}$ complexes.

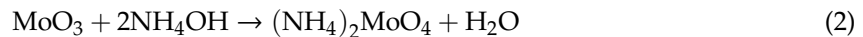
2. Materials and Methods

2.1. Powders Synthesis

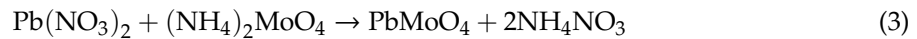
Low radioactivity ancient Pb (T2FA, Lemer Pax, France) has been used for detector shielding in AMORE [22] and other rare event search experiments [27]. Moreover, this Pb has been utilized for the fabrication of a low radioactivity Pb–Sn alloy, which serves as soldering material in the cryogenic detector construction for AMORE. Modern Pb is known to have an internal activity of tens-thousands Bq/kg from ^{210}Pb [28]. Radioactivity of an ancient Pb was investigated recently by a cryogenic detection technique, which is most sensitive for this measurement and ^{210}Pb concentration was reported to be lower than 715 $\mu\text{Bq/kg}$ [27]. Such a low activity of the ancient Pb is quite encouraging for its utilization in PMO synthesis. For this purpose, the ancient Pb block was cut in small pieces, cleaned by HNO_3 , and dried. The dried Pb pieces were used to synthesize two different batches of PMO powders by the wet chemistry technique. The first batch of PMO powders was synthesized from ancient Pb and commercial MoO_3 (Alfa Aesar) while the second batch was from ancient Pb and deeply purified MoO_3 powders. The purification procedure and its intrinsic radioactivity results are published elsewhere in [29]. First, $\text{Pb}(\text{NO}_3)_2$ was synthesized by following the chemical reaction presented in Equation (1):



Second, ammonium molybdate solution was prepared following Equation (2).



An extra amount of MoO_3 (5% by weight) compared with the theoretical requirement according to Equation (3) was used to synthesize PMO. The solution of $\text{Pb}(\text{NO}_3)_2$ was added dropwise to the solution of $(\text{NH}_4)_2\text{MoO}_4$ under continuous stirring with a magnetic stirrer. Immediately, white powders were precipitated. The powders were collected and dried at 550°C in vacuum to be used for crystal growths.



An extra amount of molybdenum remains in NH_4NO_3 solution, which was recovered from the waste solution by adjusting the pH of the solution to 2, using HNO_3 acid. A detailed description of the PMO powder synthesis procedure is illustrated in Figure 1.

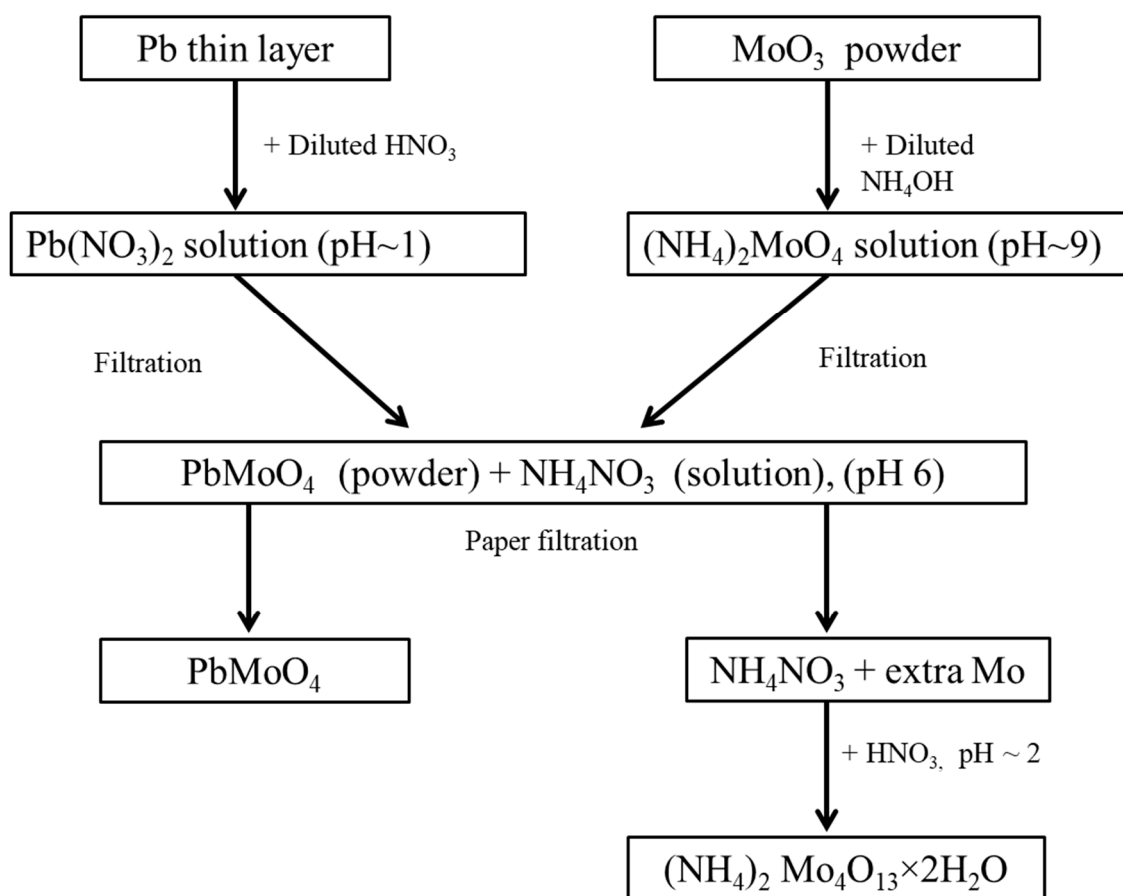


Figure 1. Flow chart of the necessary steps employed for the synthesis of PMO powder.

2.2. Crystal Growth

A conventional Czochralski method was used for the growth of PMO crystals from the synthesized powders. The first batch of PMO powders was loaded into a platinum crucible having both a diameter and height of 3 cm. The crucible was transferred to a Czochralski crystal growth chamber and the powders were melted with radio frequency heating in an Ar atmosphere. Temperature was monitored using a thermocouple attached to the bottom of the crucible and controlled by temperature controllers. After complete melting, a PMO seed was slowly lowered to the melt and the crystal was grown with the pulling and rotation rates of 1 mm/h and 10 rpm, respectively. Grown PMO crystals from the first and second batches of powders with diameter of ~15 mm and length of 40 mm are shown in Figure 2.

During crystal growth, a slight evaporation of MoO_3 was observed due to its higher vapor pressure than PbO at the elevated temperature [5].

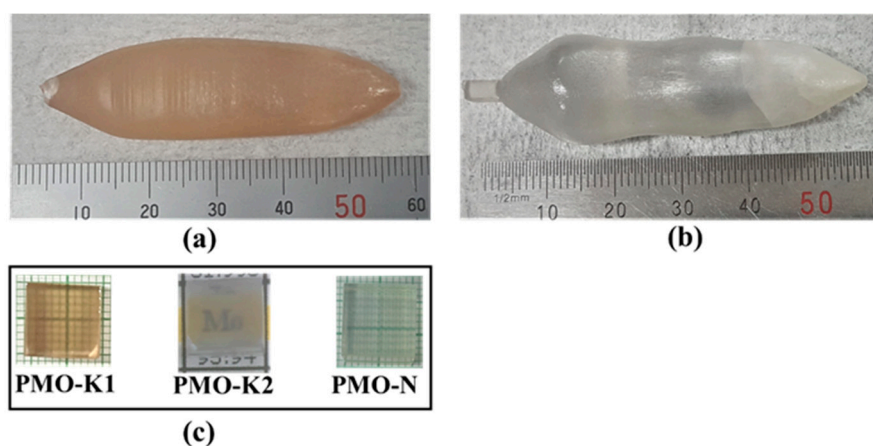


Figure 2. Photographs of the PMO crystals grown from (a) the first batch, (b) second batch of synthesized powders, and (c) 10 mm \times 10 mm \times 10 mm polished samples from crystals grown from the first and second batch powders and that received from NIIC.

The PMO crystal grown from the first batch of powders had a dark yellowish color (Figure 2a) due to the low purity of MoO_3 powders. This coloration effect in the PMO crystal was previously studied with different purity grade starting materials and attributed to impurities present in the starting materials [13]. The impurities' concentrations for the grown crystal were not measured. Nevertheless, in analogy, we assume that this coloration is due to the same origin. Our assumption is further supported from the colorless PMO crystal (Figure 2b) grown from the second batch of powders that was prepared from the ancient Pb and deeply purified MoO_3 powders. Samples with dimensions of 10 mm \times 10 mm \times 10 mm were cut from the grown crystals using a diamond coated stainless steel wire saw and optically polished for various characterizations. The grown crystals were compared with a 10 mm \times 10 mm \times 10 mm PMO sample from the Nikolaev Institute of Inorganic Chemistry (NIIC), which was grown by the low thermal gradient Czochralski technique from commercially available modern PbO and sublimed MoO_3 powders. The samples grown at our laboratory from the first and second batch powders and from the NIIC were labeled as PMO_K1, PMO_K2, and PMO_N, respectively as shown in Figure 2c.

2.3. Characterizations

The grown PMO crystals were characterized by x-ray powder diffraction (XRD) analysis for confirmation of the phase using an XPERT-MED diffractometer. X-rays with a wavelength of 0.154 nm were generated from a Cu target with power of 40 kV and current of 30 mA. The XRD data were collected in the 2θ range of $10\text{--}70^\circ$ with a step size of 0.025° and scanning rate of 3 s/step. The recorded XRD data of the PMO crystals were refined by the Rietveld refinement method using Material Analysis Using Diffraction (MAUD) software [30]. Luminescence of the grown crystals were measured in the temperature range of 10–300 K using an excitation of 4.42 eV from a light emitting diode (LED) source. The crystal samples were wrapped from three sides with several layers of 250 μm thick Teflon tape to improve light collection while the other three faces were kept bare for thermal coupling to the Cu sample holding plate, incident light from the excitation source, and emission light collection, respectively. Emitted lights from the crystal were collected through a quartz light guide by a calibrated QE65000 ocean optics fiber spectrometer. A schematic representation of the low temperature experimental setup used for the luminescence measurement of the PMO crystal is shown in Figure 3a. The scintillation light yields of the grown and reference crystals were measured in the temperature range of 10–300 K under 662 keV γ -ray excitations from a ^{137}Cs source. Four faces of the crystal sample except the bottom

for thermal coupling and top for light collection were wrapped with several layers of Teflon tape and placed in the cryostat. The ^{137}Cs source was also placed inside the cryostat at ~ 1 cm from the sample. Temperature of the sample was monitored by a thermal sensor attached to the bottom of the sample holding the Cu plate. The temperature stability of the sample was also confirmed in a separate measurement by a thermal sensor attached directly to the top of the sample. A schematic representation of the low temperature scintillation measurement setup is presented in Figure 3b. Lights from the crystals were fed to a XP2260 PMT through a quartz light guide fixed at the center of the cylindrical cryostat as shown in Figure 3. The PMT was located at a fixed position outside the cryostat at room temperature and operated at -2.2 kV for all the measurements. Signals from PMT were digitized with a 400 MS/s FADC in a time window of $64 \mu\text{s}$. An offline analysis of the recorded data was performed for scintillation light yield with a customized C++ code compiled and run in ROOT [31]. The systematic error in light yield from the position dependence of the sample during several measurements was calculated to be $\leq 7\%$, as reported in our previous work [20]. For the thermally stimulated luminescence (TSL) measurement, the crystal sample was cooled down to 10 K and irradiated by x-rays generated from a Cu anode through the beryllium (Be) window. After irradiation, the sample was heated at a rate of 0.1 K/s and the TSL intensity through the XP2260 PMT was recorded by a homemade counter in the temperature range of 10–300 K. The schematic representation of the TSL measurement setup is shown in Figure 3c.

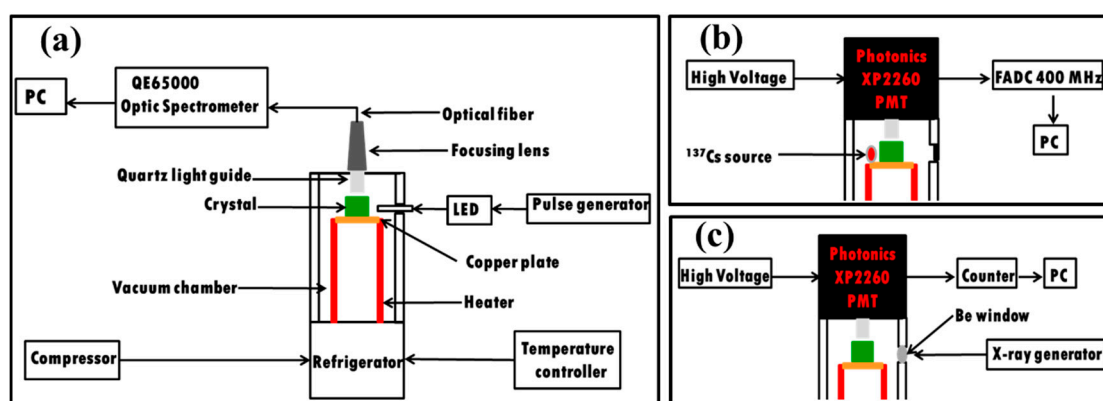


Figure 3. Schematic representations of the low temperature experimental setups used for (a) luminescence, (b) scintillation, and (c) thermoluminescence measurements of the PMO crystals.

3. Results

The XRD results of the grown crystals measured at room temperature together with those fitted with the Rietveld refinement method are shown in Figure 4a,b. The Rietveld refinement results show good agreements between experimental data and theoretical results (Figure 4a,b). The residues in Figures represent differences between experimental XRD profile and calculated data which are very close to zero in intensity scale. The Goodness of Fit (GOF) is defined as:

$$\text{GOF} = \frac{wR_p}{R_{\text{exp}}}, \quad (4)$$

where wR_p and R_{exp} are weighted and expected profile residuals, respectively. wR_p and R_{exp} are calculated from the Rietveld refinement of the measured powder XRD data of the PMO crystals. These parameters are mentioned in Figure 4a,b, respectively, and used to calculate the GOF. Details about the Rietveld refinement method can be found elsewhere in [32]. The wR_p values were less than 9% for both PMO crystals, which are in the acceptable ($wR_p < 10\%$) range for a medium complex phase such as tetragonal [14]. Moreover, the GOF of 1.09 and 1.15 were obtained for PMO-K1 and PMO-K2, respectively, showing good quality of the refinement. PMO crystallizes in the scheelite type tetragonal structure with the space group $I4_1/a$ with obtained lattice parameters of $a = 5.439 \text{ \AA}$, $c = 12.112 \text{ \AA}$ for

PMO-K1 and $a = 5.437 \text{ \AA}$, $c = 12.114 \text{ \AA}$ for PMO-K2, which are in good agreement with previously reported values [14]. A detail description about the structural refinement of PMO crystals grown with various methods can be found elsewhere in [14].

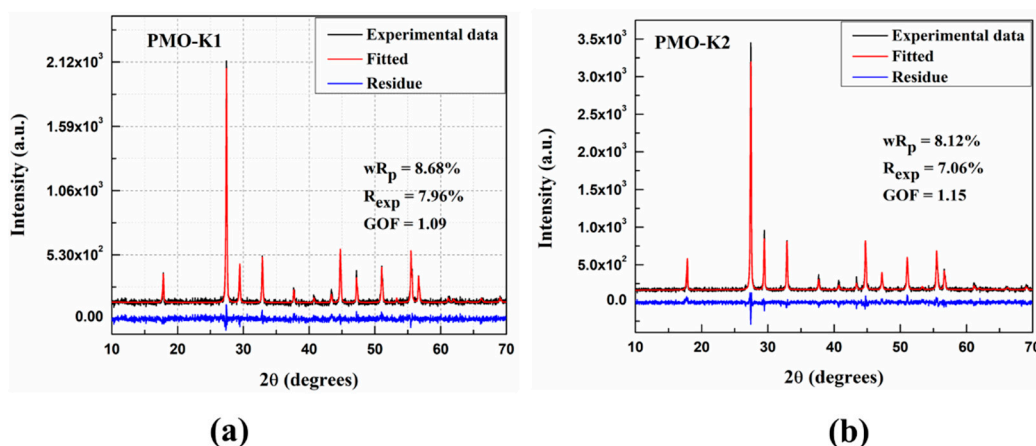


Figure 4. XRD patterns of (a) PMO-K1 and (b) PMO-K2 crystals.

Emission spectra of the grown PMO crystals at various temperatures are shown in Figure 5a,b. Under excitation with 4.42 eV lights, these crystals showed weak luminescences at 200 K. Decreasing temperatures of the crystals enhanced luminescence having the highest intensity at 10 K (Figure 5a,b). Emission spectra observed in this study have similar bands as those reported earlier in studies with different excitation energies [19,33,34]. The emission spectra are composed of overlapping emission bands as shown in Figure 5c. Deconvolution of the 420–900 nm band in the emission spectrum of PMO-K2 at 10 K shows two emission bands with the maximum peaks at 515 nm and 575 nm, respectively. These emission bands originated from degenerated triplet states $^3T_{1,2} \rightarrow ^1A_1$ transitions of MoO_4^{2-} oxyanionic complexes. A short wavelength band at about 402 nm was from the $^1T_{1,2} \rightarrow ^1A_1$ singlet transition of the MoO_4^{2-} complex [34]. Temperature dependence of the integrated luminescence intensities of PMO-K1, PMO-K2, and PMO-N measured under the same experimental conditions are shown in Figure 5d. Luminescence intensities of all these crystals decreased upon increasing temperature at above 75 K. Moreover, luminescence light yields at 10 K for PMO-K1 and PMO-K2 were measured to be 70% and 100%, respectively, to that of PMO-N. The decrease in luminescence intensity with the increase in crystal temperature are assigned to the effect of thermal quenching due to the dominant non-radiative recombination process at high temperatures. The significance of non-radiative recombination processes reduces at low temperatures and results in an enhancement of light yield [16,35].

The temperature dependence of scintillation light yield under excitation with 662 keV γ -rays from a ^{137}Cs source is shown in Figure 6a for PMO_N and PMO_K2. The photopeak in pulse height distribution like the one shown in Figure 6b was fitted with a Gaussian function at each temperature and the mean channel number is plotted as a function of temperature.

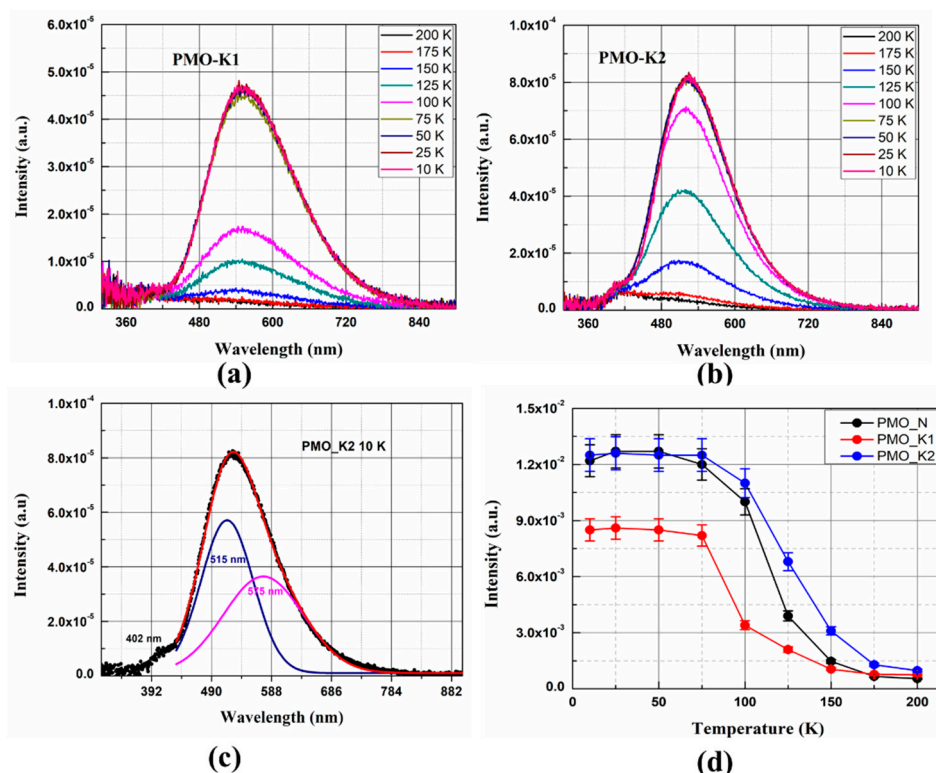


Figure 5. (a,b) Emission spectra of PMO-K1 and PMO-K2 at different temperatures, (c) emission spectrum of PMO-K2 at 10 K deconvoluted by two Gaussian distribution functions, and (d) temperature dependences of integrated luminescence intensities of PMO-K1 (red circles), PMO-K2 (blue circles) and PMO-N (black circles). All the measurements were performed under 4.42 eV excitation from an LED source.

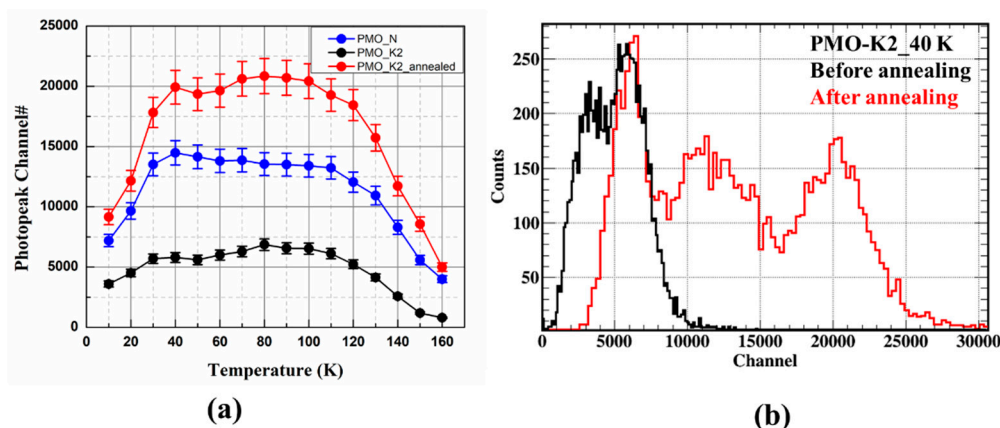


Figure 6. (a) Temperature dependence of scintillation light yields of PMO-K2 before (red circles) and after annealing (blue circles) in an air atmosphere and PMO-N (black circles), (b) pulse height distribution of PMO-K2 before (black) and after annealing (red) measured at 40 K. All these measurements were performed under 662 keV γ -ray excitation from a ^{137}Cs source.

Light outputs were compared with PMO-N at all temperatures (Figure 6a). Due to the poor scintillation light output of PMO_K1, only comparisons of PMO_K2 and PMO_N are presented in the rest of this manuscript. The temperature dependence of light yield has a similar tendency for both PMO_N and PMO_K2 crystals (i.e., enhanced up to 40 K and then quenched upon further cooling the crystals down to 10 K). Light yield of PMO-K2 at 10 K was calculated to be 50% of PMO-N before annealing. Growths of PMO crystals in an Ar atmosphere create oxygen deficiencies. These oxygen

deficiencies act as electron trapping centers and reduce light yield when the PMO crystal is excited by high energy photons. Therefore, annealing of the PMO-K2 crystal at 900 °C for 24 hours in an air atmosphere reduced the concentration of oxygen deficiencies, resulting in the enhancement of light output to 127% of PMO-N at 10 K. As presented in Figure 6b, light output shows an enhancement by a factor of ~ 3.3 at 40 K after annealing. The decrease in scintillation light yield below 40 K can be understood from the TSL glow curve. As can be seen from the TSL glow curve in Figure 7, measured after x-ray irradiation at 10 K, multiple traps at 39 K, 73 K, and 106 K were observed like that reported earlier for a PMO crystal [25]. The origin of these trap centers was investigated extensively by the electron paramagnetic resonance (EPR) technique and high energy photon irradiation and reported in [25,36,37]. The high intensity peak at ~ 40 K, below which the light yield reduced significantly, was assigned to the trapping of electrons at $(\text{MoO}_4)^{2-}$ oxyanionic complexes [25]. Energy transfer to the luminescence center was strongly influenced by the charge carriers trapping at the trap centers. From the temperature dependence of the integrated luminescence intensity under a 4.42 eV excitation (direct creation of excitons), no quenchings at low temperatures were observed. However, light outputs under high energy 662 keV γ -ray excitations showed a steep drop below 40 K due to the presence of trap centers at low temperatures. These trap centers are in competition with the radiative recombination of charge carriers and responsible for the quenching of light yield below 40 K [25].

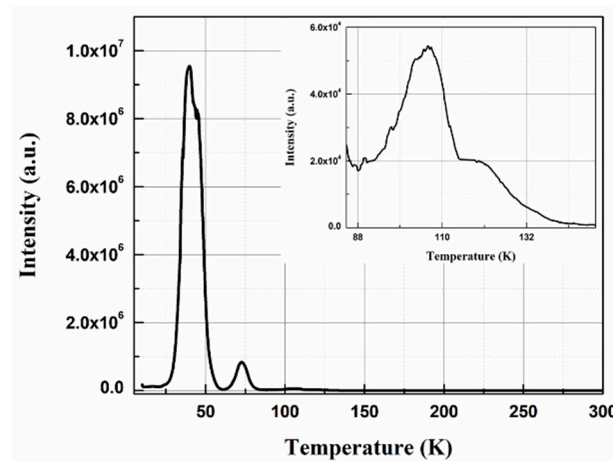


Figure 7. TSL glow curve of PMO-K2 measured after x-ray irradiation at 10 K and measured at heating rate of 0.1 K/s. The inset shows an enlarged view of 80–150 K region.

To qualitatively analyze the internal activities from ^{210}Pb , internal background measurements were carried out at 50 K over six hours for PMO_K2 and PMO_N at the low temperature experimental setup. As shown in Figure 8a, the internal background peak of 5.3 MeV α was detected from ^{210}Po for PMO-N, which contains modern Pb. A similar internal background of a 5.3 MeV α peak from ^{210}Po was reported elsewhere in [20] for a PMO crystal grown from a modern Pb. However, a signature of such background peak was not observed for PMO-K2 (Figure 8b) from this data, showing a preliminary evidence of low radioactivity of this crystal for ^{210}Pb , as expected. This measurement does not provide a quantitative internal activity of this crystal, therefore, a more detailed investigation will be carried out at mK temperature in a CPSD setup and will be reported elsewhere.

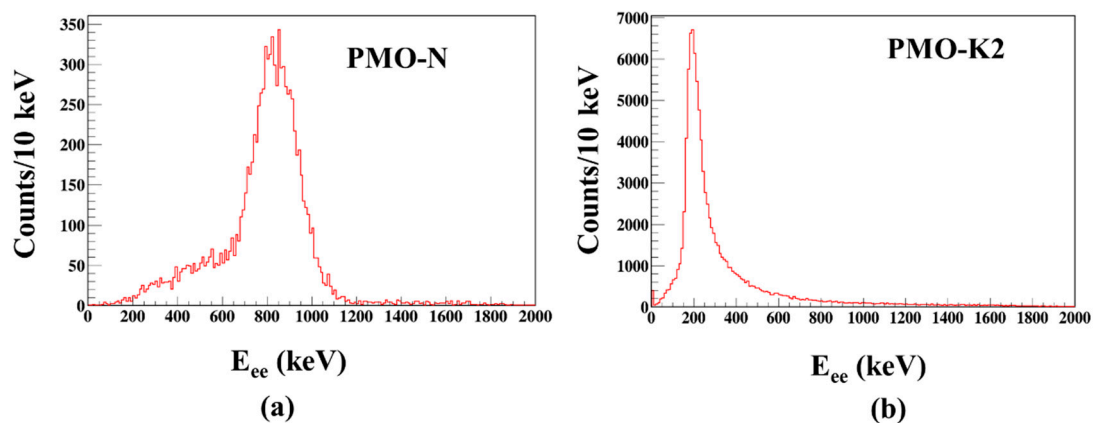


Figure 8. Total background spectra of (a) PMO-N and (b) PMO-K2 measured at 50 K over six hours.

4. Conclusions

A synthesis method for PMO powders from ancient Pb and deeply purified MoO₃ powders was successfully developed. A single crystal growth from the synthesized powders by the Czochralski technique resulted in crack free optically good quality PMO crystals. The grown crystals showed a high phase purity as confirmed from powder XRD measurement. The dark yellowish colored and colorless PMO crystals grown from commercial grade and deeply purified powders, respectively, and confirmed that the origins of colors were due to impurities. Low temperature luminescence measurements revealed the identical emission bands due to singlet T_{1,2} and triplet T_{1,2} states to the ground state ¹A₁ transition of the (MoO₄)²⁻ complex, as reported previously. Scintillation light yields of PMO-K2 after annealing in an air atmosphere under 662 keV γ -ray excitations in low temperatures from 10 to 160 K were higher than those in the reference PMO crystal. Moreover, the quenching of scintillation light yield below 40 K was confirmed from the TSL measurement due to the presence of high intensity glow peak at low temperature and attributed to the trapping of charge carriers at these trap centers. An internal background measurement of PMO-K2 at 50 K showed a low activity in ²¹⁰Pb. These investigations reveal great potential for PMO to be used for 0 ν $\beta\beta$ decay search in ¹⁰⁰Mo. Further study on the PMO crystal as a bolometer at mK temperature is underway to fully investigate its feasibility for the 0 ν $\beta\beta$ decay search.

Author Contributions: Conceptualization, A.K., P.A., and H.K.; Methodology, A.K. and P.A.; Validation, A.K. and H.K.; Formal analysis, A.K.; Investigation, A.K. and H.K.; Resources, H.K.; Data curation, A.K.; Writing—original draft preparation, A.K. and M.H.L.; Writing—review and editing, H.K., P.A., and M.H.L.; Visualization, A.K. and H.K.; Supervision, H.K.; Project administration, H.K.; Funding acquisition, H.K. and Y.K., All authors have read and agreed to the published version of the manuscript.

Funding: These investigations were funded by the Ministry of Science and Technology, Korea (MEST) (No. 2018R1A2A1A05022079) and IBS-R016-D1-2018-a01.

Conflicts of Interest: The authors declare no conflicts of interest.

References

- Chesler, R.B.; Pinnow, D.A.; Benson, W.W. Suitability of PbMoO₄ for Nd: YAIG Intracavity Acoustooptic Modulation. *Appl. Opt.* **1971**, *10*, 2562. [[CrossRef](#)] [[PubMed](#)]
- Damen, E.P.N.; Arts, A.F.M.; De Wijn, H.W. High-frequency monochromatic acoustic waves generated by laser-induced thermomodulation. *Phys. Rev. Lett.* **1995**, *74*, 4249–4252. [[CrossRef](#)] [[PubMed](#)]
- Hernández-Uresti, D.B.; Martínez-de la Cruz, A.; Torres-Martínez, L.M. Photocatalytic properties of PbMoO₄ synthesized by co-precipitation method: Organic dyes degradation under UV irradiation. *Res. Chem. Intermed.* **2012**, *38*, 817–828. [[CrossRef](#)]
- Takano, S.; Esashi, S.; Mori, K.; Namikata, T. Growth of high-quality single crystals of lead molybdate. *J. Cryst. Growth* **1974**, *24–25*, 437–440. [[CrossRef](#)]

5. Sabharwal, S.C.; Sangeeta; Desai, D.G. Investigations of single crystal growth of PbMoO_4 . *Cryst. Growth Des.* **2006**, *6*, 58–62. [[CrossRef](#)]
6. Senguttuvan, N.; Moorthy Babu, S.; Dhanasekaran, R. Some aspects on the growth of lead molybdate single crystals and their characterization. *Mater. Chem. Phys.* **1997**, *49*, 120–123. [[CrossRef](#)]
7. Shlegel, V.N.; Borovlev, Y.A.; Grigoriev, D.N.; Grigorieva, V.D.; Danevich, F.A.; Ivannikova, N.V.; Postupaeva, A.G.; Vasiliev, Y.V. Recent progress in oxide scintillation crystals development by low-thermal gradient Czochralski technique for particle physics experiments. *J. Instrum.* **2017**, *12*, C08011. [[CrossRef](#)]
8. Chen, H.; Ge, C.; Li, R.; Wang, J. Bridgman growth of lead molybdate crystals. *J. Mater. Sci.* **2006**, *41*, 5383–5385. [[CrossRef](#)]
9. Senguttuvan, N.; Moorthy Babu, S.; Subramanian, C. Synthesis, crystal growth and mechanical properties of lead molybdate. *Mater. Sci. Eng. B* **1997**, *47*, 269–273. [[CrossRef](#)]
10. Lim, L.C.; Tan, L.K.; Zeng, H.C. Bubble formation in Czochralski-grown lead molybdate crystals. *J. Cryst. Growth* **1996**, *167*, 686–692. [[CrossRef](#)]
11. Sangeeta; Desai, D.G.; Singh, A.K.; Tyagi, M.; Sabharwal, S.C. Non-stoichiometry-induced cracking in PbMoO_4 crystals. *J. Cryst. Growth* **2006**, *296*, 81–85. [[CrossRef](#)]
12. Zeng, H.C. Correlation of PbMoO_4 crystal imperfections to Czochralski growth process. *J. Cryst. Growth* **1997**, *171*, 136–145. [[CrossRef](#)]
13. Tyagi, M.; Singh, S.G.; Singh, A.K.; Gadkari, S.C. Understanding colorations in PbMoO_4 crystals through stoichiometric variations and annealing studies. *Phys. Status Solid Appl. Mater. Sci.* **2010**, *207*, 1802–1806. [[CrossRef](#)]
14. Bomio, M.R.D.; Cavalcante, L.S.; Almeida, M.A.P.; Tranquilin, R.L.; Batista, N.C.; Pizani, P.S.; Li, M.S.; Andres, J.; Longo, E. Structural refinement, growth mechanism, infrared/Raman spectroscopies and photoluminescence properties of PbMoO_4 crystals. *Polyhedron* **2013**, *50*, 532–545. [[CrossRef](#)]
15. Mikhailik, V.B.; Kraus, H. Performance of scintillation materials at cryogenic temperatures. *Phys. Status Solid Basic Res.* **2010**, *247*, 1583–1599. [[CrossRef](#)]
16. Babin, V.; Bohacek, P.; Bender, E.; Krasnikov, A.; Mihokova, E.; Nikl, M.; Senguttuvan, N.; Stolovits, A.; Usuki, Y.; Zazubovich, S. Decay kinetics of the green emission in tungstates and molybdates. *Radiat. Meas.* **2004**, *38*, 533–537. [[CrossRef](#)]
17. Nagornaya, L.L.; Danevich, F.A.; Dubovik, A.M.; Grinyov, B.V.; Henry, S.; Kapustyanyk, V.; Kraus, H.; Poda, D.V.; Kudovbenko, V.M.; Mikhailik, V.B.; et al. Tungstate and molybdate scintillators to search for dark matter and double beta decay. *IEEE Trans. Nucl. Sci.* **2009**, *56*, 2513–2518. [[CrossRef](#)]
18. Nagorny, S.; Pattavina, L.; Kosmyrna, M.B.; Nazarenko, B.P.; Nisi, S.; Pagnanini, L.; Pirro, S.; Schaffner, K.; Shekhovtsov, A.N. PbMoO_4 scintillating bolometer as detector to searches for the neutrinoless double beta decay of ^{100}Mo . *J. Phys. Conf. Ser.* **2017**, *841*, 012025. [[CrossRef](#)]
19. Khan, A.; Daniel, D.J.; Kim, H.; Pandey, I.R.; Shlegel, V.; Lee, M.H.; Kim, Y. Luminescence and scintillation characterization of PbMoO_4 crystal for neutrinoless double beta decay search. *Radiat. Meas.* **2019**, *123*, 34–38. [[CrossRef](#)]
20. Danevich, F.A.; Grinyov, B.V.; Henry, S.; Kosmyrna, M.B.; Kraus, H.; Krutyak, N.; Kudovbenko, V.M.; Mikhailik, V.B.; Nagornaya, L.L.; Nazarenko, B.P.; et al. Feasibility study of PbWO_4 and PbMoO_4 crystal scintillators for cryogenic rare events experiments. *Nucl. Instrum. Methods Phys. Res. Sect. A Accel. Spectrom. Detect. Assoc. Equip.* **2010**, *622*, 608–613. [[CrossRef](#)]
21. Kim, G.B.; Choi, S.; Danevich, F.A.; Fleischmann, A.; Kang, C.S.; Kim, H.J.; Kim, S.R.; Kim, Y.D.; Kim, Y.H.; Kornoukhov, V.A.; et al. A CaMoO_4 crystal low temperature detector for the AMoRE neutrinoless double beta decay search. *Adv. High. Energy Phys.* **2015**, *2015*, 1–15. [[CrossRef](#)]
22. Jo, H.S.; Choi, S.; Danevich, F.A.; Fleischmann, A.; Jeon, J.A.; Kang, C.S.; Kang, W.G.; Kim, G.B.; Kim, H.J.; Kim, H.L.; et al. Status of the AMoRE Experiment Searching for Neutrinoless Double Beta Decay Using Low-Temperature Detectors. *J. Low Temp. Phys.* **2018**, 1–8. [[CrossRef](#)]
23. Armengaud, E.; Augier, C.; Barabash, A.S.; Bellini, F.; Benato, G.; Benoît, A.; Beretta, M.; Bergé, L.; Billard, J.; Borovlev, Y.A.; et al. The CUPID-Mo experiment for neutrinoless double-beta decay: Performance and prospects. *Eur. Phys. J. C* **2020**, *80*, 1–15. [[CrossRef](#)]
24. Pandey, I.R.; Karki, S.; Kim, H.J.; Kim, Y.D.; Lee, M.H.; Ivannikova, N.V. Luminescence and Scintillation properties of novel disodium dimolybdate ($\text{Na}_2\text{Mo}_2\text{O}_7$) single crystal. *IEEE Trans. Nucl. Sci.* **2018**, *65*, 2125–2131. [[CrossRef](#)]

25. Spassky, D.A.; Nagirnyi, V.; Mikhailin, V.V.; Savon, A.E.; Belsky, A.N.; Laguta, V.V.; Buryi, M.; Galashov, E.N.; Shlegel, V.N.; Voronina, I.S.; et al. Trap centers in molybdates. *Opt. Mater.* **2013**, *35*, 2465–2472. [[CrossRef](#)]
26. Spassky, D.A.; Kozlova, N.S.; Nagirnyi, V.; Savon, A.E.; Hizhnyi, Y.A.; Nedilko, S.G. Excitation energy transfer to luminescence centers in MIIMoO_4 (MII = Ca, Sr, Zn, Pb) and Li_2MoO_4 . *J. Lumin.* **2017**, *186*, 229–237. [[CrossRef](#)]
27. Pattavina, L.; Beeman, J.W.; Clemenza, M.; Cremonesi, O.; Fiorini, E.; Pagnanini, L.; Pirro, S.; Rusconi, C.; Schäffner, K. Radiopurity of an archaeological Roman lead cryogenic detector. *Eur. Phys. J. A* **2019**, *55*, 127. [[CrossRef](#)]
28. Danevich, F.A.; Kim, S.K.; Kim, H.J.; Kim, Y.D.; Kobychyev, V.V.; Kostezh, A.B.; Kropivnyansky, B.N.; Laubenstein, M.; Mokina, V.M.; Nagorny, S.S.; et al. Ancient Greek lead findings in Ukraine. *Nucl. Instrum. Methods Phys. Res. Sect. A Accel. Spectrom. Detect. Assoc. Equip.* **2009**, *603*, 328–332. [[CrossRef](#)]
29. Karki, S.; Aryal, A.; Gileva, O.; Kim, H.J.; Kim, Y.; Lee, D.Y.; Park, H.K.; Shin, K. Reduction of radioactive elements in molybdenum trioxide powder by sublimation method and its technical performance. *J. Instrum.* **2019**, *14*, T11002. [[CrossRef](#)]
30. Lutterotti, L.; Matthies, S.; Wenk, H.R.; Schultz, A.S.; Richardson, J.W. Combined texture and structure analysis of deformed limestone from time-of-flight neutron diffraction spectra. *J. Appl. Phys.* **1997**, *81*, 594–600. [[CrossRef](#)]
31. Brun, R.; Rademakers, F. ROOT—An object oriented data analysis framework. *Nucl. Instrum. Methods Phys. Res. Sect. A Accel. Spectrom. Detect. Assoc. Equip.* **1997**, *389*, 81–86. [[CrossRef](#)]
32. Sahu, N.; Panigrahi, S. Mathematical aspects of Rietveld refinement and crystal structure studies on PbTiO_3 ceramics. *Bull. Mater. Sci.* **2011**, *34*, 1495–1500. [[CrossRef](#)]
33. Groenink, J.A.; Blasse, G. Some new observations on the luminescence of PbMoO_4 and PbWO_4 . *J. Solid State Chem.* **1980**, *32*, 9–20. [[CrossRef](#)]
34. Kajitani, T.; Itoh, M. Time-resolved composite nature of the self-trapped exciton luminescence in PbMoO_4 . *Phys. Status Solidi Curr. Top. Solid State Phys.* **2011**, *8*, 108–111. [[CrossRef](#)]
35. Mihokova, E.; Nikl, M.; Bohacek, P.; Babin, V.; Krasnikov, A.; Stolovich, A.; Zazubovich, S.; Vedda, A.; Martini, M.; Grabowski, T. Decay kinetics of the green emission in $\text{PbWO}_4:\text{Mo}$. *J. Lumin.* **2003**, *102*, 618–622. [[CrossRef](#)]
36. Buryi, M.; Laguta, V.; Fasoli, M.; Moretti, F.; Jurek, K.; Trubitsyn, M.; Volnianskii, M.; Nagorny, S.; Shlegel, V.; Vedda, A.; et al. Charge trapping processes and energy transfer studied in lead molybdate by EPR and TSL. *J. Lumin.* **2019**, *205*, 457–466. [[CrossRef](#)]
37. Buryi, M.; Laguta, V.; Fasoli, M.; Moretti, F.; Trubitsyn, M.; Volnianskii, M.; Vedda, A.; Nikl, M. Electron self-trapped at molybdenum complex in lead molybdate: An EPR and TSL comparative study. *J. Lumin.* **2017**, *192*, 767–774. [[CrossRef](#)]

